ECCOMAS Congress 2016
VII European Congress on Computational Methods in Applied Sciences and Engineering
M. Papadrakakis, V. Papadopoulos, G. Stefanou, V. Plevris (Eds.)
Crete Island, Greece, 5-10 June 2016

A NUMERICAL STUDY FOR THE BUCKLING CAPACITY OF WIND TURBINE BLADES: GEOMETRY, LOADING AND MATERIAL INFLUENCE

Efstathios E. Theotokoglou[1], Georgios Balokas[1, 2] and Evgenia K. Savvaki[1]

[1] Department of Mechanics, Laboratory of Testing and Materials
School of Applied Mathematical and Physical Sciences, National Technical University of Athens,
Athens, GR-15773 Greece
stathis@central.ntua.gr , euginias@gmail.com

[2] Structure Development Department, ELAN-AUSY GmbH
Harburger Schloßstr. 24, Hamburg, Germany
Georgios.Balokas@elan-ausy.com

Keywords: Composite materials, Wind turbine blades, Fiber-reinforced polymers, Finite element analysis, Nonlinear buckling analysis, Eigenvalue analysis

Abstract. *In this paper the composite load-carrying support structure of wind turbine blades is investigated. The buckling behavior of wind turbine blades is studied numerically by using the finite element method, as experimental experience shows that local buckling is a major failure mode that dominantly influences the total collapse of the blade. Significant advantages are derived from the combination of different fiber-reinforced polymers in hybrid material structures, but also from kevlar-fiber blades.*

1 INTRODUCTION

In recent years, wind energy has noted the highest growth rate in comparison with other renewable energy sources [1]. This is mainly due to the increasing energy needs and the simultaneous depletion of natural resources, but also to the lack of environmental hazards and the practically unlimited resources. Consequently, the exploitation of wind energy systems, e.g. wind turbines, forms an industry domain that gathers strong interest in both research and construction activities. The need to optimize their performance results in higher power wind turbines with significantly longer blades and innovative features in terms of geometry and materials.

The blades are perhaps the most critical structural members of the wind turbine, since the increasing diameter of the rotor brings many challenges to the surface, regarding the design and construction. The wind turbine blade (WTB) is essentially a cantilever beam mounted on a rotating hub with key design criteria the high stiffness, the low weight and the aerodynamic shape. These features are covered by fiber-reinforced composite materials. Such fiber-reinforced polymer materials are implemented in laminates and sandwich structures for the outer aerodynamic shell, but also for the internal load-carrying structure, ensuring the required strength and stiffness of the blade.

In this paper the support structure is investigated for the case of a hollow one-piece construction cross-section (box girder). Through parametric analyses an attempt was made to investigate the buckling behavior of the load-carrying box girder due to flap-wise bending, with respect to the following parameters: the geometry, the loading imposition and the material properties. This study offers a clear perspective about the buckling capacity and its sensitivity on the parameters mentioned above, but also about the post-buckling behavior of the models. Furthermore, this investigation leads to useful conclusions for the material design optimization of the load-carrying box girder, as significant advantages are derived from the combination of different fiber-reinforced polymers in hybrid material structures, but also from kevlar-fiber blades.

2 NUMERICAL MODELING AND ANALYSIS

2.1 Geometrical model

There are currently two major types of configuration for the internal geometry of the blade, which differ in terms of design and connection to the outer shell. The first case is the so-called two-piece construction and consists of two distinct vertical stiffness joints, known as shear-webs, which extend along the blade and provide the required internal support. The second case is the so-called one-piece construction and is extensively studied in the present paper. Here, the internal support of the blade is provided by a single hollow section structure, which extends almost to the entire length of the blade and is usually called box girder. The tension and the compression flange of this structure are welded to the upwind and downwind outer shell respectively. The parts welded to the shell are called spar-caps and they are linked to the shear-webs, which are placed vertically in the cross-section, at 15% and 50% of the length of the chord c, as measured from the leading edge of the blade (Fig.1).

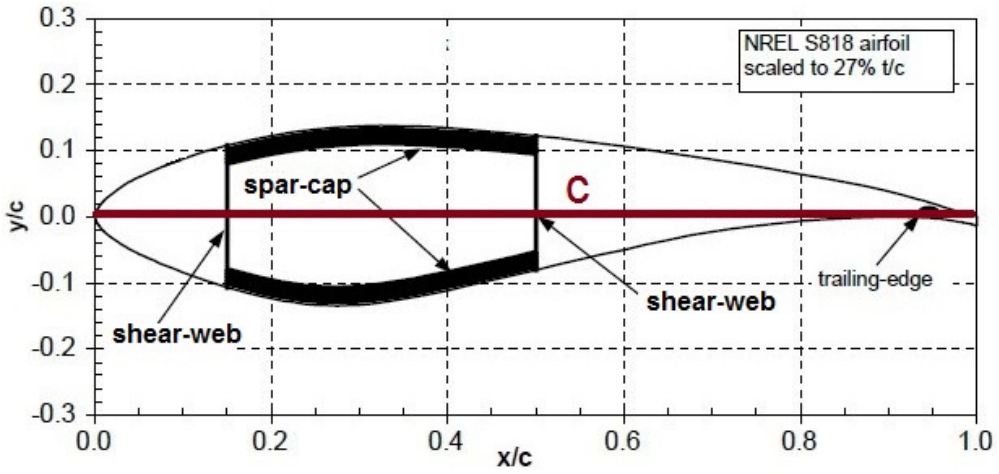

Figure 1: Cross-section of the blade for the one-piece construction case [2]

The box girder provides the required strength and stiffness of the outer shell of the blade, both locally and globally. For this reason, the box girder was chosen to be studied separately, since the dominant deformation mode is almost identical to the one of the blade, while the increased slenderness of the panels makes it sensitive to local buckling phenomena. Experimental data show that local (or shear) buckling is a major failure mode that significantly influences the total collapse of the blade [3-5].

The present study models the internal load-carrying box girder of a horizontal axis wind turbine, with nominal power 1MW, 64.14m tower and 63.04m rotor diameter, for the case of a single box-like, hollow section internal support. The total length of the blade, (from the rotational axis to the blade tip) equals to 30m. The blades are divided into three sections, depending on the deformation levels due to the stress loads [2]. In our case, the root segment is 2.10m long (equal to 7% of the blade length), the transition segment 5.40m (equal to 18% of the blade length) and the main box girder segment 22.50m, inside of which the internal support mechanism is located (hatched area in Fig. 2).

For the numerical analysis, a finite element code was developed, using the ANSYS 14.5 software [6]. The analysis parameters chosen were: a) the geometry of the cross-section, b) the simulation of the flap-wise loading and c) the fiber-reinforced composite material properties. In all cases both linear and nonlinear buckling analyses were performed. From the latter, the respective equilibrium paths (load-displacement curves) were extracted.

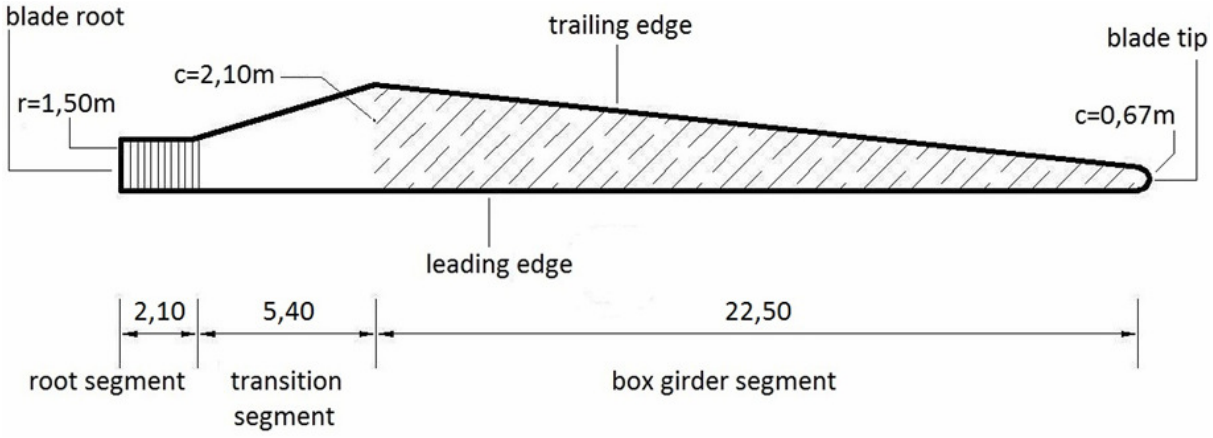

Figure 2: Division of the blade [5].

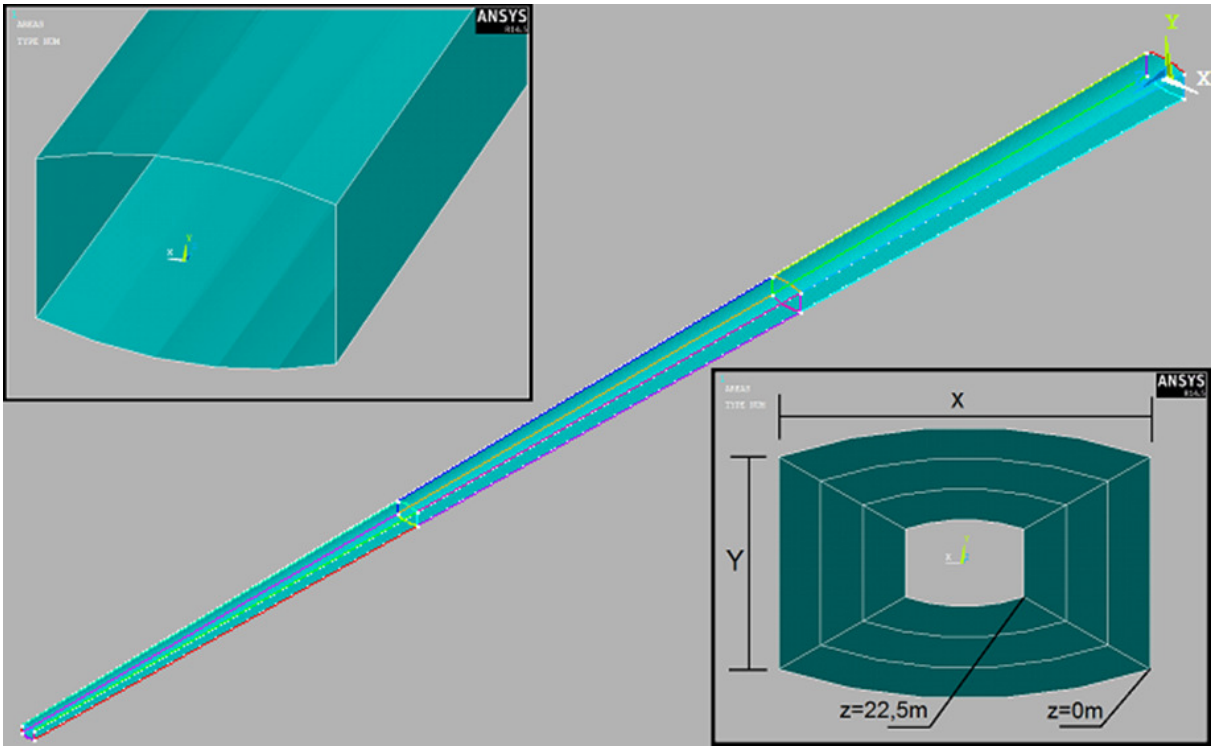

Figure 3: Geometrical model.

The dimensions and the design details of the examined blade correspond to the S818 airfoil model [2]. The coordinates of 24 points (6 for each of the 4 cross-sections) were calculated at the beginning (location z=0.0m), the end (location z=22.5m) and two intermediate positions of the box girder. Then the finite element model was constructed by presuming linear longitudinal tapering (Fig. 3). During the designing process, it is assumed double symmetry conditions for the cross section with respect to the axes X and Y, which in fact is not entirely true, as it can be shown in Figure 1. However it is acceptable, since the same assumption is made in relevant studies of the literature [3].

Shell elements were used (shell281 in ANSYS [6]) for the simulation, which are the most common type of finite elements in WTB analysis. A mesh convergence study was conducted, in order to determine the size of the finite elements for which satisfactory accuracy is achieved within reasonable computing time. So for the discretization of the models, shell elements with side length equal to 300mm were considered.

As it is obvious from Figure 3, the FE model was initially designed with the assumption of an angle formed in the transition area from the spar-cap to the shear-web. This assumption is adopted in similar studies [7]. However, it is not completely realistic since there is some curvature in the transition area. This happens in order to achieve a smooth transition to the thinner shear-web and to avoid high stress concentration. The technique applied in similar cases in composites is called “ply-drop analysis” and is implemented with gradual termination of some layers in the required region that leads to thickness reduction [3, 5, 8].

Ply-drop analysis cannot be applied efficiently in a macro-scale level, so in this study a small curvature was given as a simplistic alternative (Fig. 4a), at the initial corner of the spar-cap (Fig. 4b). This modification in the cross section design was used as an analysis parameter, in order to determine whether a small variation of the geometry of the model could affect the buckling load and the deformation of the panels.

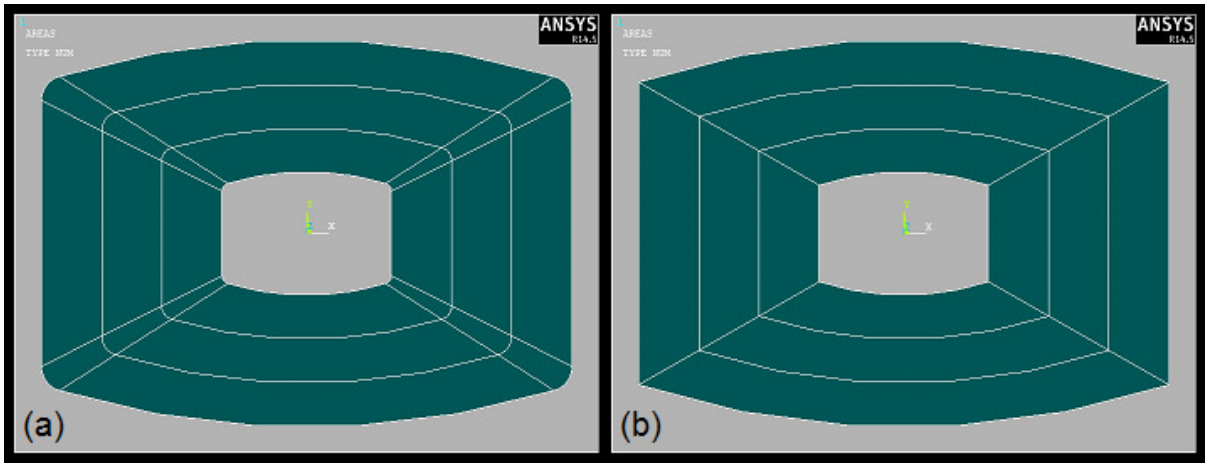

Figure 4: FEA model at the z=0.0m location: a) with curvature and b) without curvature at the transition area.

2.2 Boundary and loading conditions

There are two types of bending for the WTB: the edge-wise bending, which is vertical to one of the two edges of the blade (leading edge and trailing edge) and is caused by the gravity loads of the blade and the flap-wise bending, that is caused by the wind loads and is vertical to the large surface of the blade. Based on the global coordinate system shown in Figure 3, the edge-wise bending takes place around the Y-axis and the flap-wise around the X-axis. The blade also endures centrifugal forces due to the rotation of the rotor, although they are not significant and are usually neglected in the analysis.

In this study, four different loading simulations were examined in order to determine whether there is an influence in the critical buckling load and in the size and shape of the deformations. Moreover, in case of similar results we could reach to a conclusion regarding the most inexpensive performance.

All of our load alternatives cause flap-wise bending to the box girder, because it is the most critical condition and the one that usually leads to failure at local and/or global level [3, 9]. Specifically, the load was simulated with: a) uniform pressure, vertically spaced at the upper spar-cap (red lines matrix in Figure 5a), b) linear load along the model imposed in the middle of the upper spar-cap (Fig. 5b), c) concentrated load at the free end of the model acting on the middle of the spar-cap (Fig. 5c) and d) two concentrated loads of equal magnitude at locations z = 7.5m and z = 15m (Fig. 5d). All the loads are static, imposed by an incremental step-by-step process (Newton-Raphson method) and are applied in a way that the upper spar-cap is tensioned (upwind) and the lower spar-cap is compressed (downwind).

Regarding the boundary conditions, all four sides of the cross section at the z=0 location, are assumed fully fixed (restrained rotation and displacement of the axes X, Y and Z).

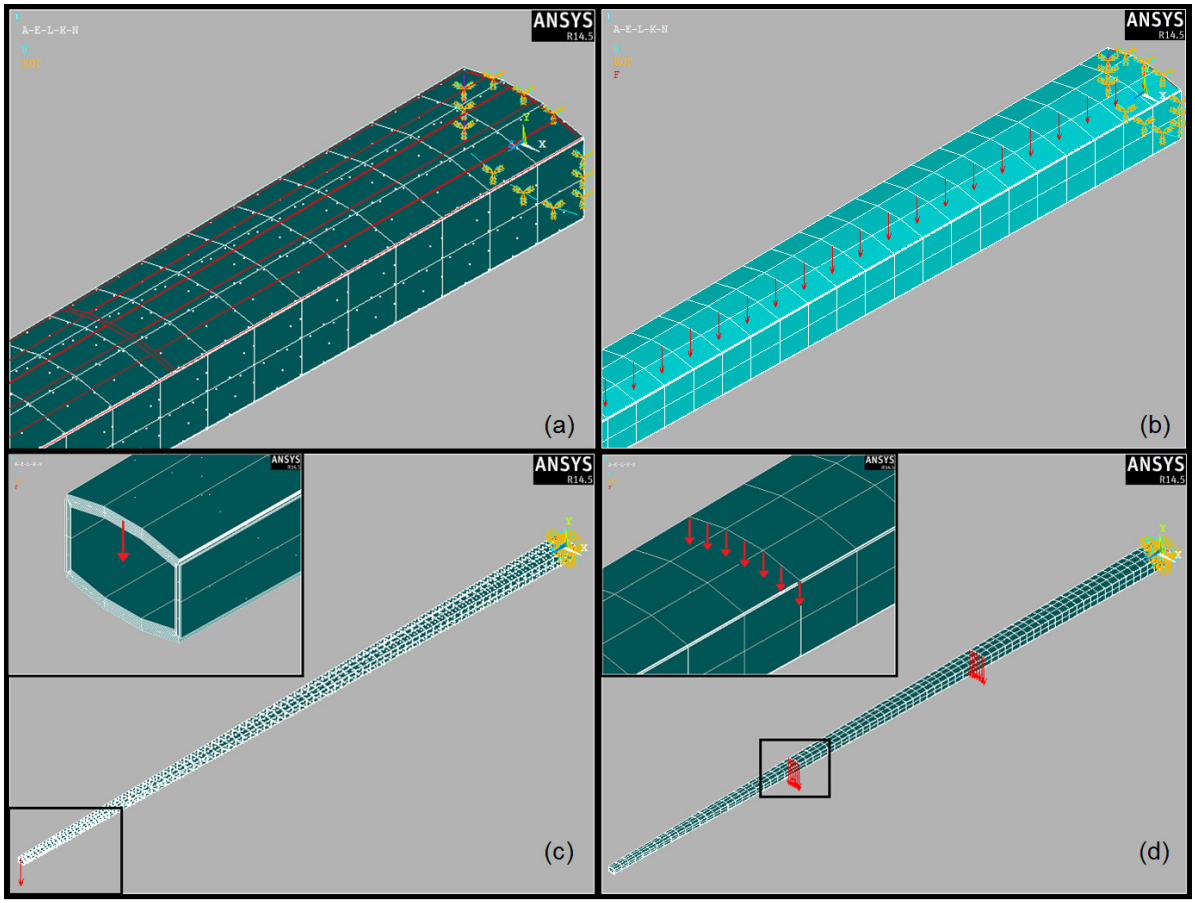

Figure 5: The four different load simulations.

2.3 Design and Material selection

The selection of appropriate materials, which can optimally cover the increasing requirements of safety, efficiency and service life of a modern, high-power, wind turbine, is perhaps the most critical task and also a great challenge for the designers. The selected materials should have three basic properties: i) high material stiffness, to maintain the optimal aerodynamic shape of the blade, but also to prevent contact with the turbine tower and local buckling phenomena, ii) low density in order to minimize the gravity loads and iii) long fatigue life to reduce material degradation during the operation and to ensure at least a 20-year service life [10].

For the blade construction, polymers reinforced with glass fibers (glass fiber reinforced plastics-GFRP) or carbon fibers (carbon fiber reinforced plastics-CFRP) are commonly used. The high-strength fibers operate as reinforcement and are retained by load bearing mean, the matrix, which is usually made of epoxy, because of its excellent properties. Such materials are light and additionally, their fibers have a much higher strength-to-weight ratio and stiffness-to-weight in comparison with steel or wood, which were initially used for blade manufacturing.

The outer airfoil skins are sandwich structures while the internal load-carrying box girder combines laminate with sandwich layup. Specifically, spar-caps are consisted of alternating equal thickness layers of triaxial laminates (-45°/0°/45°), and unidirectional laminates. The unidirectional laminates are providing the required bending stiffness, while laminates with fibers at ±45° direction are providing torsional stiffness and buckling resistance for the surface under compression. Shear-webs are constructed using a sandwich-like material consisting

of triaxial composite laminate face sheets separated by a balsa wood core. The application of a core material increases locally the bending strength and buckling resistance. The layer order is shown in Figure 6, while the identification number of each material is provided in Table 1, along with the thickness of the corresponding layer.

The thickness of the spar-caps is constant along the blade length and equal to 21.6mm, while the thickness of the shear-webs is 17.69mm at the z=0m location and 12.92mm at the z=22.5m location (linear reduction as a function of the chord length).

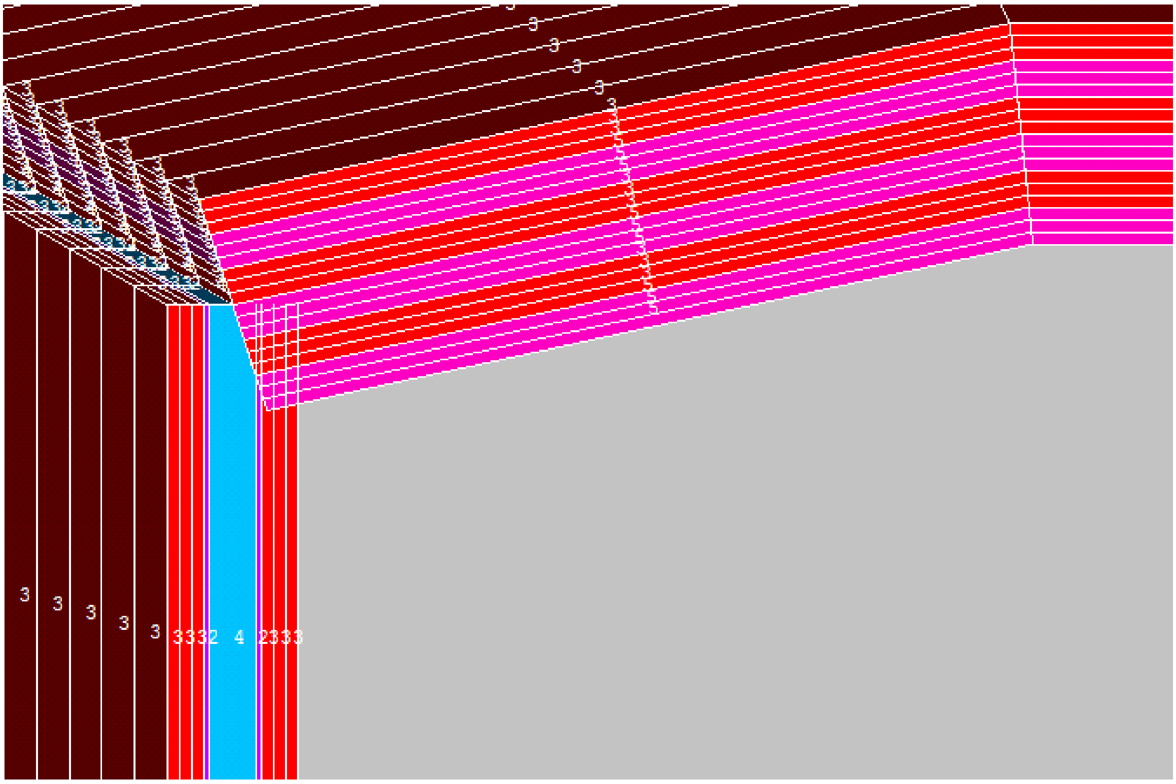

Figure 6: Model layup for the laminate structure of the spar-cap and the sandwich structure of the shear-web.

Material number	Material	Layer thickness (mm)
1	gel	0.68
2	Random material	0.59
3	Tri-axial material	1.20
4	Balsa core	0.005×chord length *c*
5	Uni-axial material	1.20

Table 1: Composite laminate layup identification and thickness

In this analysis, a comparison was conducted between three different fiber-reinforced composites: a) polymer with electrical glass fibers (GFRP), b) polymer with carbon fibers (CFRP), c) polymer with aramid fibers (AFRP) but also combination of the above in hybrid models. In all cases, the same epoxy-based matrix was used, as well as the same layup in the spar-caps and shear-webs.

Glass fibers are currently the most widely used fibers for blade construction. They are available in various types and different chemical compositions, but E-glass fibers are those primarily used for the blades, due to their mechanical performance and resistance to corrosion. However, limited information is available on the structural design process of blades (i.e. properties, layup and layer thickness), since the information remains confidential between the manufacturers. Therefore the material properties of the GFRP model, such as the thickness, sequence and orientation of individual layers were obtained from a previous study [5] and have derived from experimental results for the given fiber orientations and arrangement of materials used in another experimental study [11]. The properties of the GFRP as well as those of the core material are provided in Table 2, where E_{xx} is the axial Young's modulus, E_{yy} is the transverse Young's modulus, G_{xy} is the in-plane shear modulus, ν_{xy} is the Poisson's ratio, v_f is the fiber volume fraction, w_f is the fiber weight fraction, and ρ is the density.

Properties	Uni-axial (#5)	Tri-axial(#3)	Ran-dom (#2)	Balsa (#4)	Gel (#1)	Epoxy adhesive
E_{xx} (GPa)	31.00	24.20	9.65	2.07	3.44	2.76
E_{yy} (GPa)	7.59	8.97	9.65	2.07	3.44	2.76
G_{xy} (GPa)	3.52	4.97	3.86	0.14	1.38	1.10
ν_{xy}	0.31	0.39	0.30	0.22	0.30	0.30
u_f	0.40	0.40	-	-	-	-
w_f	0.61	0.61	-	-	-	-
ρ (g/cm^3)	1.70	1.70	1.67	0.14	1.23	1.15

Table 2: GFRP Material properties.

The size growth and the decreasing cost of carbon fibers have made them quite popular in the last 10-15 years. Carbon fibers present an exceptional combination of high stiffness, high strength and low density. Overall, they have much better performance than glass fibers, but yet they are of limited use because of their higher cost. In this study, the material properties of CFRP were obtained by applying formulas of composite materials theory [12] due to lack of experimental data similar to those used for the GFRP model. For our calculations we used the properties of AS4-D carbon fibers type and the same epoxy-based as the one used in the GFRP model. The properties of CFRP are shown in Table 3.

Properties	Uni-axial	Tri-axial	Random
E_{xx} (GPa)	146.00	65.00	62.47
E_{yy} (GPa)	18.53	22.50	62.47
G_{xy} (GPa)	9.41	13.46	24.19
ν_{xy}	0.27	0.29	0.29

Table 3: CFRP material properties.

In recent years aramid fibers are widely used, replacing metallic and inorganic fibers in composite structures in aerospace, maritime and automobile industry. Aramid fibers not only have better material properties than steel and glass fibers for the same weight level, but also maintain these properties at high temperatures, since they have high thermal insulation and fire resistance. Furthermore, aramid fiber reinforced polymers are proven to have much higher tensile strength and better resistance to fatigue from polymers with glass fibers [13]. Despite the positive characteristics that they present and their wide range of applications, the possibility of using them in WTBs manufacturing has not yet been examined. This paper investigates their buckling capacity, compared to glass and carbon fiber reinforced polymers, as they were presented above.

Aramid presents many valuable properties, depending on the treatment and the application in hand. One of its most popular derivatives is Kevlar, which is the trade name for aramid. There are many Kevlar fiber categories like Kevlar 29, Kevlar 49, Kevlar 68, Kevlar 119, Kevlar 129 and Kevlar 149. Kevlar 149 is one of the most recent categories in the Kevlar family. They have much higher Young's modulus than Kevlar fibers 29 and 49, while having approximately the same density and diameter, but a very low sensitivity to moisture (they are mainly used in aerospace). Because of these properties, Kevlar fibers 149 were chosen to be used for the fiber-reinforced polymer of the internal load carrying box girder. The mechanical properties of AFPR model were obtained by applying the same formulas used in the CFRP model and they are shown in Table 4.

Properties	Uni-axial	Tri-axial	Random
E_{xx} (GPa)	113	50.87	48.88
E_{yy} (GPa)	15.24	18.28	48.88
G_{xy} (GPa)	7.46	10.72	18.63
ν_{xy}	0.37	0.34	0.31

Table 4: AFRP material properties.

3 ANALYSIS RESULTS

3.1 Finite element analysis

We initially present the analysis results for the model considered: the E-GFRP model without curvature at the transition area between the spar-cap and the shear-web, where the load is simulated with uniform pressure vertically spaced at the upper spar-cap. We performed both eigenvalue and nonlinear buckling analysis for the baseline case as well as for all the other cases.

Eigenvalue analysis (linear buckling analysis) offers a quick estimate about the response of the model, while a rough value of the critical buckling load is calculated. The critical buckling load was estimated through linear analysis equal to 12.47KPa. However no information regarding the size of deformations or the post-buckling response of the model can be derived from the linear analysis. Moreover, linear analysis is insufficient for reaching precise conclusions because it is based on the assumption of small displacements and does not take into account the influence of nonlinear phenomena (large deformations, imperfections etc.). The most realistic behavior of the model can be obtained from the nonlinear buckling analysis. For the latter, we took into account the geometrical nonlinearity (where changes in geometry due

to large deformations significantly affect the relationship between the applied load and the displacement) and the results are presented below.

An early conclusion based on the deformed model (Fig. 7), is that the global deflection of the model is not considerably affected by local buckling. In a closer look, we can see that the local buckling area lies in the compressed spar-cap, near the root. Also, shear buckling occurs at the same position in the shear-webs. In Figure 8 the Brazier effect [8] of the blade is confirmed by the deformed shape, as the ovalization of the cross-section during buckling is apparent.

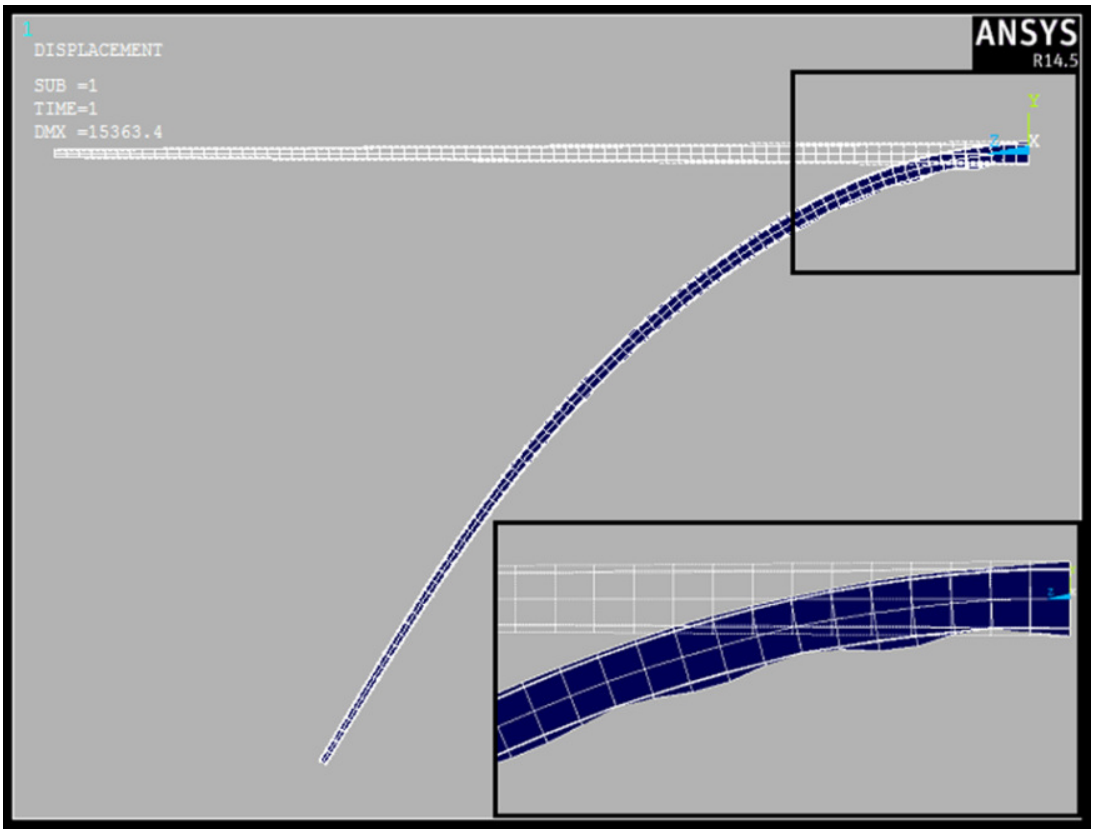

Figure 7: Global and local deformation of the model after the load imposition.

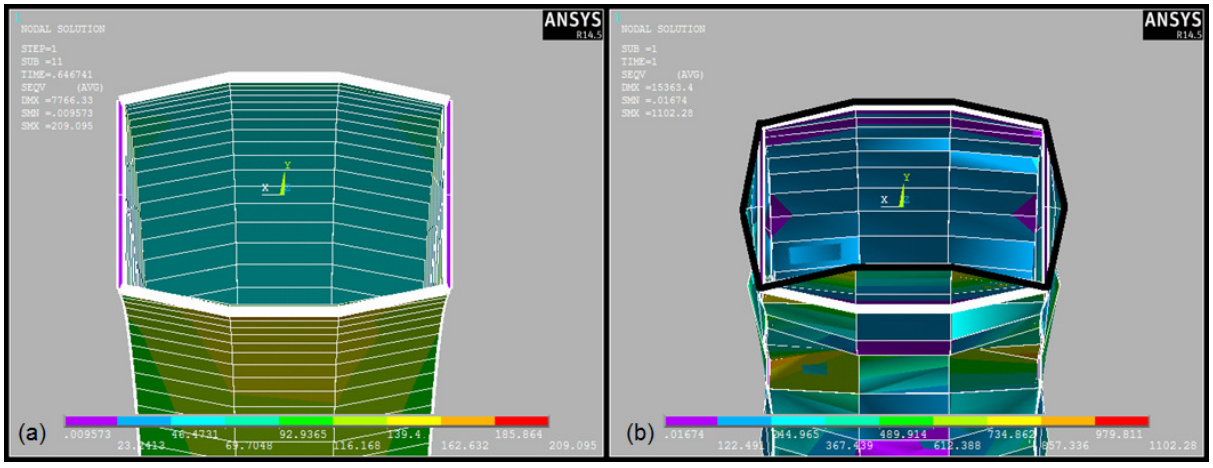

Figure 8: a) The model cross-section just before the local buckling and b) the cross-section ovalization.

The maximum local deformation (in the Y direction) of the compressed spar-cap is detected on D-spot in Fig.9 while the maximum local deformation of shear-web (in the X- direction) occurs on Z-spot in Fig. 10. The equilibrium paths are shown in Figs 11 and 12. The curves exhibit linear behavior (pre-buckling phase) up to 8.41KPa (critical buckling load), where the bifurcation point A is reached. After this point, the model has stable non-linear response, up to 13KPa (point C) (post-buckling phase).

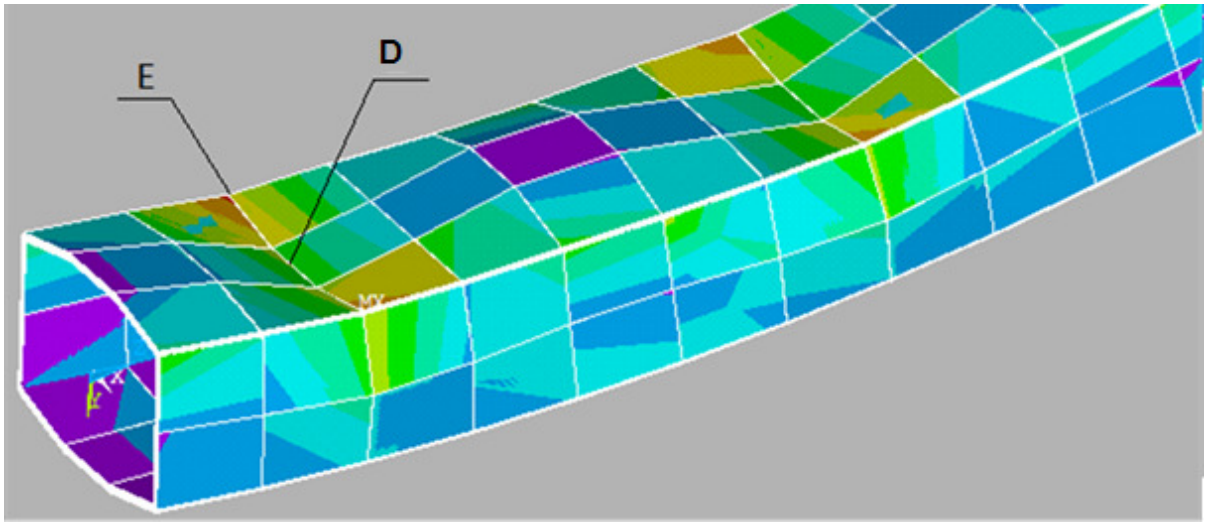

Figure 9: Spar-cap local buckling and von Mises stresses distribution

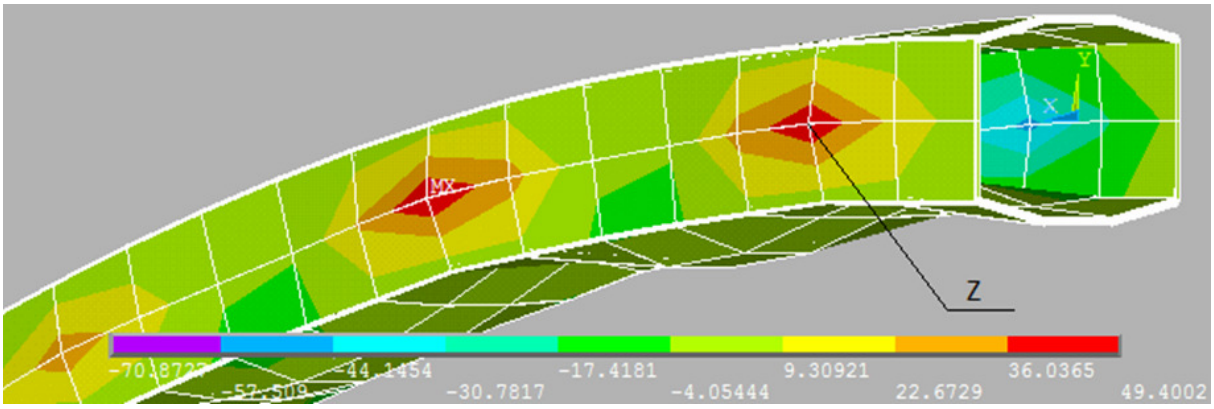

Figure 10: Displacements in the X-direction (in mm)

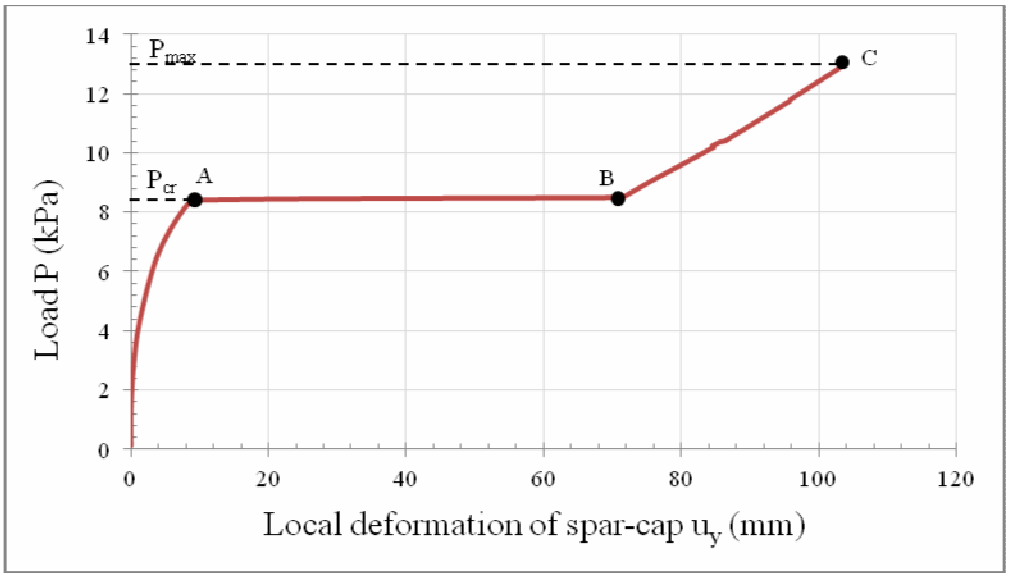

Figure 11: Load-displacement path (displacement at the Y-direction).

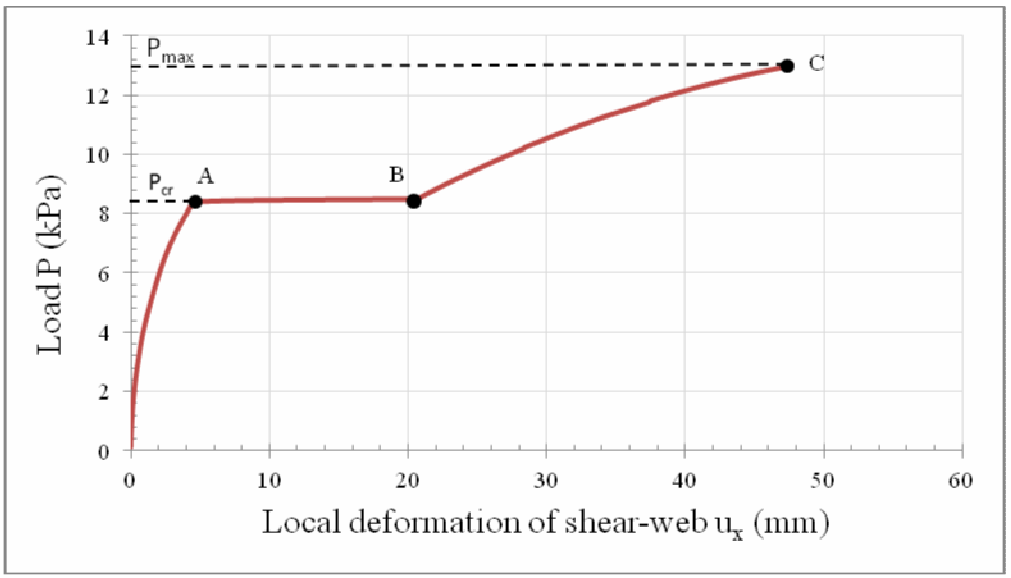

Figure 12: Load-displacement path (displacement at the X-direction).

3.2 Cross-section geometry parameter

We compare two models based on the GFRP material properties, with uniform pressure on the spar-cap and the geometrical discrepancies described in Section 2.1. From the load-displacement paths (Fig. 13), we can see that the two models have similar response both in the pre-buckling and the post-buckling phase, with equal stiffness and about the same critical buckling load. The deformed shape of both models is identical in terms of position and number of folds. However, the post-buckling path for the model with the curvature at the transition area has higher inclination and the size of deformations is smaller.

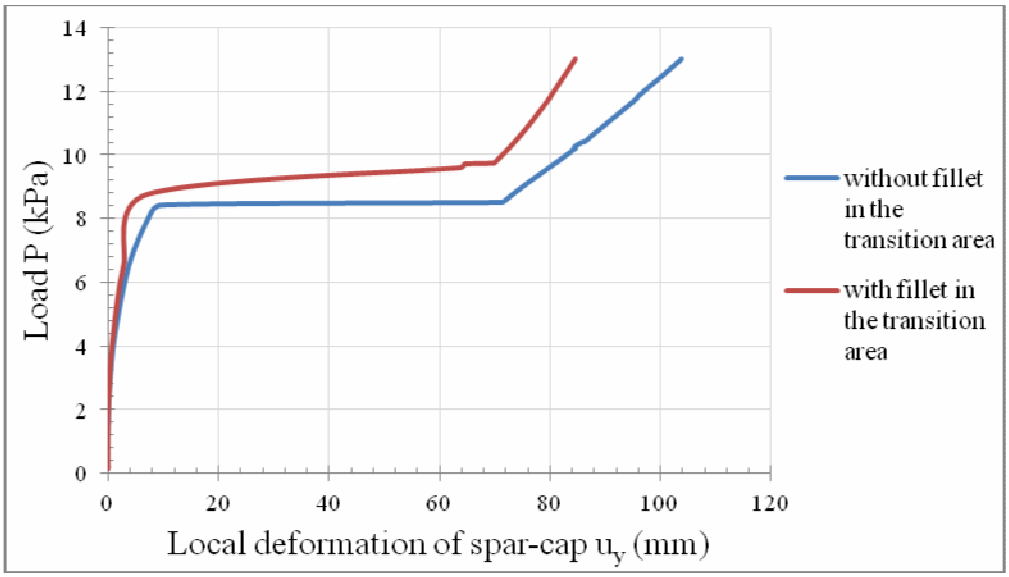

Figure 13: Load-displacement path (displacement at the Y-direction).

3.3 Loading imposition parameter

Based on specific examples of the literature [3, 9, 14], we examined four different ways of the loading simulation, which were described in Section 2.2. More specifically, except uniform pressure it is imposed: linear load in the middle of upper spar-cap of maximum value P_{max} = 6.32KN/m, concentrated load at the free end of the model of maximum value P_{max}=60KN and two concentrated loads of equal magnitude, with maximum value 63KN each. To allow comparison between pressure (KPa), linear load (KN/m) and concentrated loads (KN), we convert everything into equivalent bending moment at the support of the model for each load step.

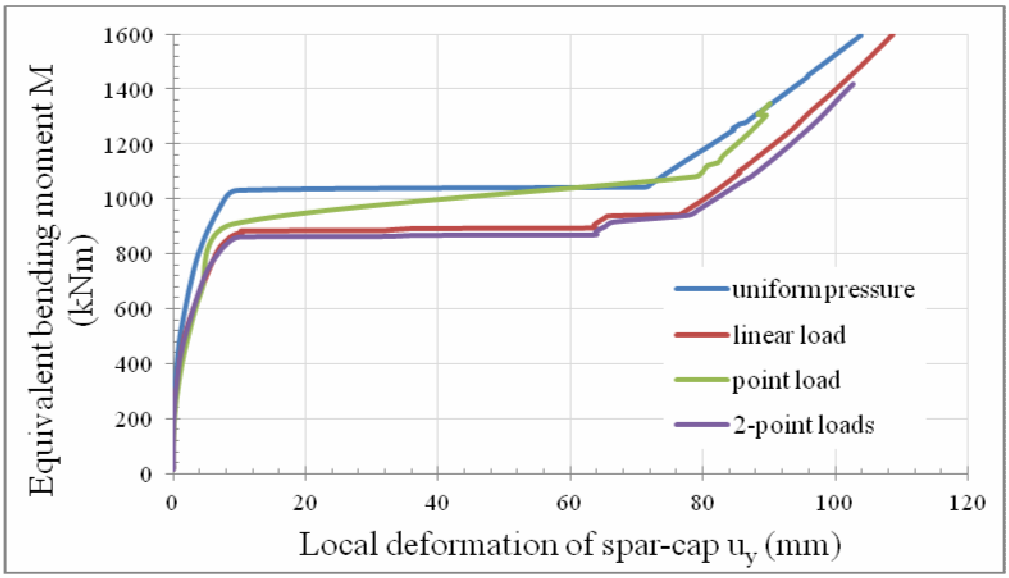

Figure 14: Load-displacement path (displacement at the Y-direction).

From Figure 14, it is clear that the models have similar behavior both in the pre-buckling and post-buckling phase. The pre-buckling paths are in general very close, while they are identical for the cases of the linear load and the two concentrated loads. However, there are

differences in the critical buckling load, where the maximum value emerged when we imposed uniform pressure. On the other hand, the critical load for the concentrated load at the free-end case is closer to the average value, while the size of the deformations is smaller. It is noted that there were no significant savings regarding computational efficiency in any of the examined cases.

Based on the above and the relatively small deviations observed, it can be deduced that the different loading simulations may indeed affect the distribution of the stresses across the model but they do not affect crucially its load carrying capacity and response. Therefore we can neither recommend nor exclude any of these load simulation methods based on our results.

3.4 Material properties parametric analysis

- **Comparison between glass, carbon and kevlar-fiber models**

The fiber-reinforced composite material properties are the last and most important analysis parameters in our study. The equilibrium paths (Fig. 15) indicate that the CFRP model has more than twice the buckling capacity of the GFRP model and also much higher stiffness (pre-buckling path with higher slope). This was expected, due to the remarkable properties of carbon. The AFRP model also has high critical buckling load and stiffness in comparison with the GFRP. Additionally, a significant restriction of deflections is observed prior the bifurcation point.

However, the AFRP model exhibits unstable post-buckling behavior, as it is indicated by the displacement values after the bifurcation point is reached. This instability can also be observed in the deformed shape of the model, as multiple deformation peaks emerge during loading history.

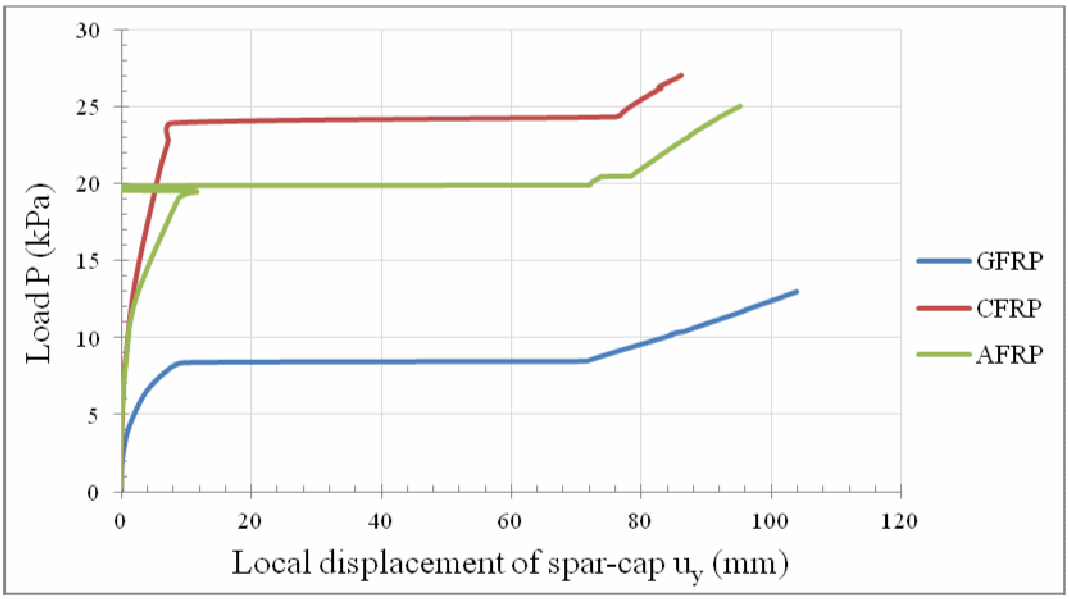

Figure 15: Load-displacement path (displacement at the Y-direction).

- **Comparison between hybrid models of GFRP and CFRP**

The need to further increase the strength-to-weight ratio and the stiffness-to-weight ratio of the blades has turned wind turbine industry towards hybrid structures. Hybrid models are likely to have higher strength and lower density compared to blades that are exclusively constructed by glass fibers. In this section, the following 3 cases are investigated: i) replacement

of the GFRP by CFRP material in the shear-webs (the GFRP_spar-cap/ CFRP_shear-web model), ii) replacement of the GFRP by CFRP material in spar-caps (the CFRP_spar-cap/ GFRP_shear-web model) and iii) replacement of the GFRP by CFRP material in the uni-axial layers in spar-caps (the CFRP_uni-axial in spar-cap model).

The nonlinear curves (Fig 16) indicate that the GFRP_spar-cap/ CFRP_shear-web has almost the same response as the GFRP model. The hybrid model has a slightly greater stiffness. The CFRP_spar-cap/ GFRP_shear-web model has exactly the same pre-buckling path as the CFRP model up to the critical buckling load. However, this model does not have an increasing post-buckling section (stiffening). The lack of sufficient post-buckling strength is a significant disadvantage. The most reasonable combination is that of the carbon fibers placed only in the uni-axial layers of the spar-caps. In this case, the hybrid model is found to have a sufficient combination of load carrying capacity and post-buckling strength, but also minimum use of the expensive carbon material. This conclusion is also reached in relevant studies of the literature [15, 16].

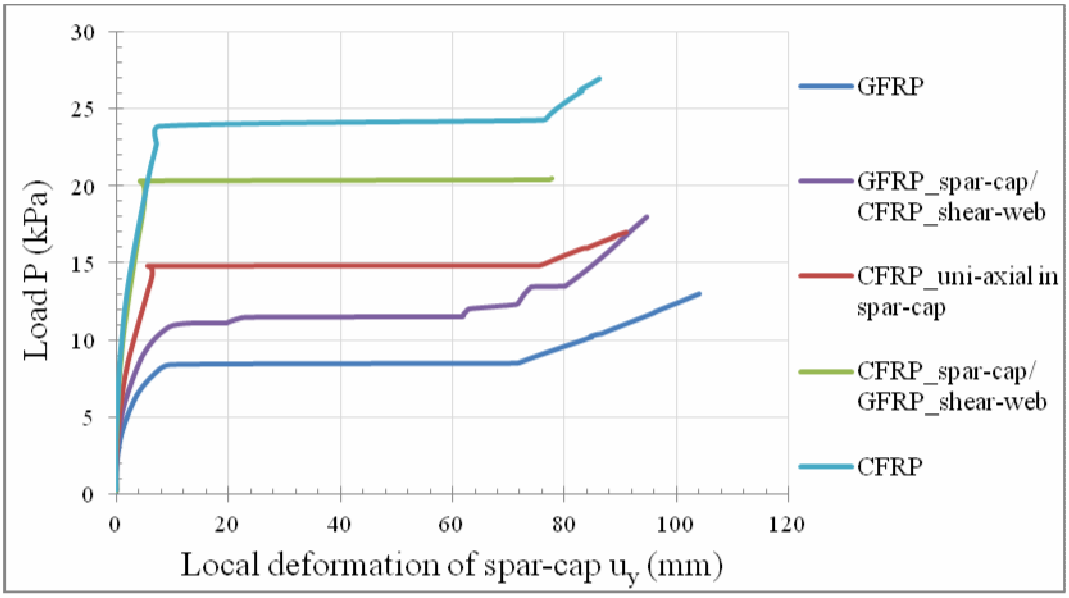

Figure 16: Load-displacement path (displacement at the Y-direction).

- **Comparison between hybrid models of CFRP and AFRP**

The response of hybrid models constructed by carbon and aramid fibers was also investigated. In particular, the following cases were studied: i) the replacement of the CFRP material by the AFRP material in spar-caps (the AFRP_spar-cap/ CFRP_shear-web model) and ii) the replacement of the CFRP by AFRP material in shear-webs (the CFRP_spar-cap/ AFRP_shear-web model).

The AFRP_spar-cap/ CFRP_shear-web model has the same curve with the AFRP model, without the unstable post-buckling behavior that the latter exhibits. This result is characterized as a positive contribution. The CFRP_spar-cap/ AFRP_shear-web model has exactly the same response, stiffness and stable post-buckling behavior as the CFRP model (their load-displacement paths are identical). Furthermore, the deformed models differ slightly (Fig. 18). Thus, the following useful conclusion results: when CFRP material is used in the spar-caps and AFRP material in shear-webs, a model can be created with the same load carrying capacity and buckling strength as the CFRP model, with significant savings in cost and weight (the Kevlar fibers 149 are cheaper and lighter than carbon fibers).

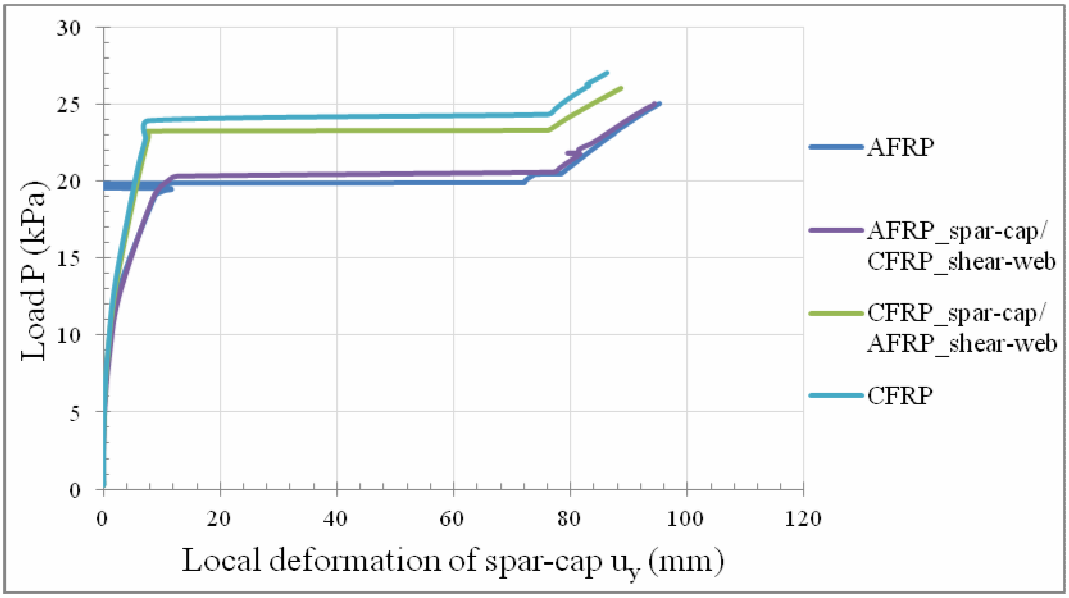

Figure 17: Load-displacement path (displacement at the Y-direction).

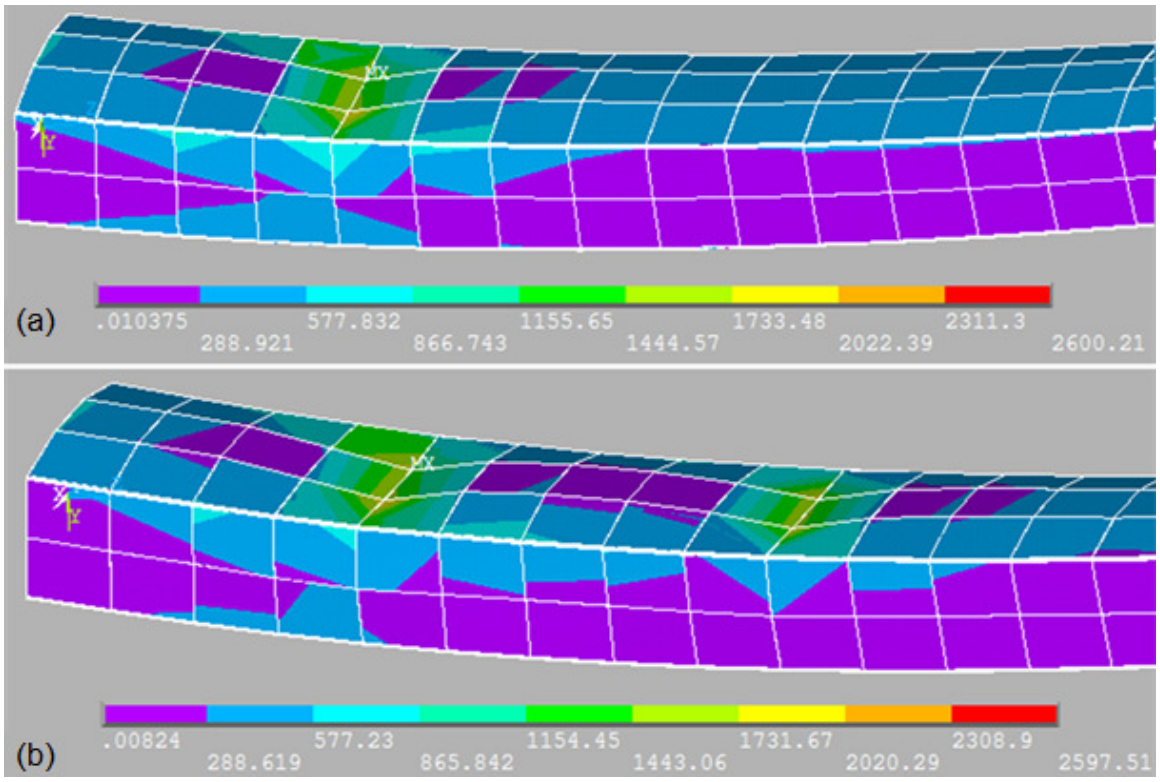

Figure 18: Local deformations and von Mises stress distribution at the critical buckling load for: a) the CFRP model and b) the CFRP_spar-cap/ AFRP_shear-web model

- **Comparison between hybrid models GFRP and AFRP**

Finally, the response of hybrid models, constructed by glass and aramid fibers, was investigated. The following cases were studied: i) the replacement of the AFRP material by the GFRP material in the spar-caps (the GFRP_spar-cap/ AFRP_shear-web model model), ii) the replacement of the GFRP by AFRP material in the spar-caps (the AFRP_spar-cap/

GFRP_shear-web model) and iii) replacement of the GFRP by AFRP material in the uni-axial layers of the spar-caps (the AFRP_uni-axial in spar-cap model).

The GFRP_spar-cap/ AFRP_shear-web model has slightly higher stiffness and critical buckling load than the GFRP model (Fig. 19). The AFRP_spar-cap/ GFRP_shear-web model exhibits sufficient load carrying capacity, without the unstable post-buckling behavior that was observed at the AFRP model analysis. The load-displacement curve for the AFRP_uni-axial in spar-cap model is in the middle of the rest, presenting a satisfatory combination of load carrying capacity and post-buckling strength. As a total conclusion from all the hybrid cases considered, it should be noted that the response and the stiffness of the hybrid models are defined by the spar-cap material.

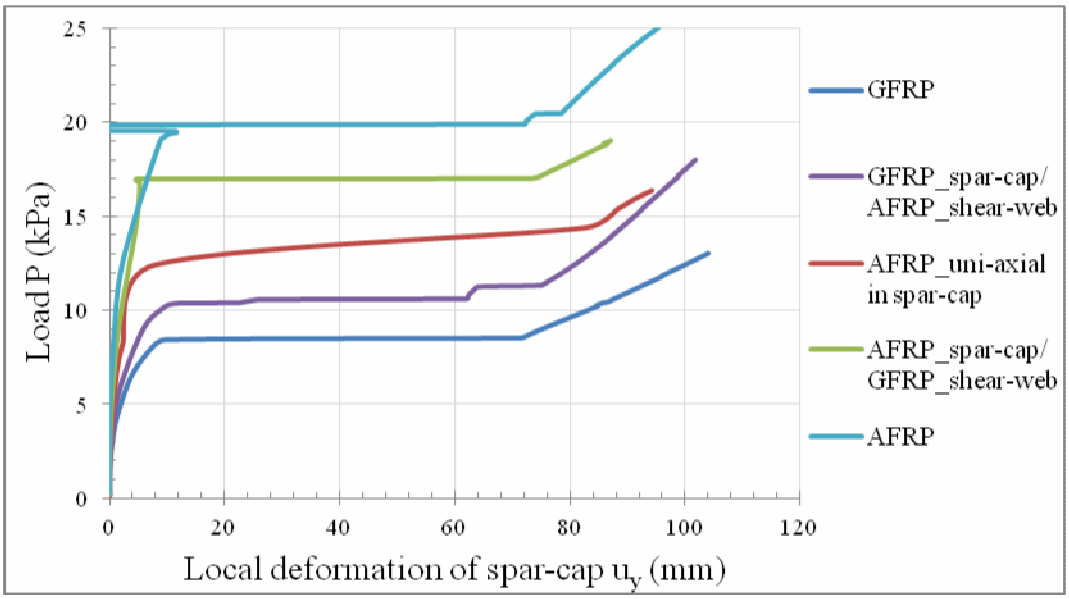

Figure 19: Load-displacement path (displacement at the Y-direction).

4 CONCLUSIONS

This paper studies the buckling capacity of the internal support of WTBs, by performing parametric analyses with respect to geometry, loading and material properties. The nonlinear buckling analysis results are consistent with a related study of the literature [3]. On the other hand, the eigenvalue analysis was proved extremely conservative, since the critical buckling load values are overestimated in all cases examined. The above confirms the necessity of the nonlinear analysis, despite the increased computational cost required. Nonlinear analysis leads to more realistic results and should always be performed in cases where changes in the geometry, due to large deformations, significantly affect the relationship between the applied load and the displacement.

The comparison between the GFRP, CFRP and AFRP models, showed that the CFRP model has greater stiffness and strength compared with the GFRP model and approximately double critical buckling load. Positive results are obtained from the use of Kevlar fibers, since the stiffness and the critical buckling load of the AFRP model is quite larger than those of the GFRP model. However, the unstable post-buckling behavior of the AFRP model is negatively evaluated. This instability is eliminated immediately, in cases where aramid fibers were used in conjunction with glass or carbon fibers in hybrid models. This is a strong prompt towards further research in the use of Kevlar fibers in wind turbine blades. Additionally, it is of great interest that if the CFRP material is used in the spar-caps and the AFRP material in shear-

webs (instead of CFRP material), a model can be produced with the same strength and buckling capacity as the CFRP material, but significantly cheaper and lighter, since the Kevlar 149 fibers have a lower cost and weight.

This study offers a clear perspective about the buckling capacity of the blade and its sensitivity when the material parameters are changed, but also about the post-buckling behavior and strength of the models. Nevertheless, there is space for improvement in the FEM simulation (e.g. more realistic configuration of the geometrical model, without the assumption of double symmetry at the X and Y axes, with more detailed ply-drop design in the transition area etc.). Further studies should also include material nonlinearity, by testing various models of plasticity for the composite fiber reinforced polymers. Moreover, the significant advantages that seemed to arise from the use of aramid fibers should be further tested, in order to examine their response in experimental models.

REFERENCES

[1] Renewable Energy Policy Network for the 21st Century, Renewables 2015 Global Status Report, Paris, France.

[2] D.A. Griffin, WindPact Turbine Design Scaling Studies Technical Area 1 - Composite Blades for 80- to 120-Meter Rotor, NREL, Washington, 2001.

[3] B.F. Sorensen, E. Jorgensen, C.P. Debel, F.M. Jensen, H.M. Jensen, T.K. Jacobsen and K.M. Halling, Improved design of large wind turbine blade of fiber composites based on studies of scale effects (Phase 1)-Summary Report, Risø-R-1390(EN), Risø National Laboratory, Roskilde, Denmark, 2004.

[4] O.T. Thomsen, Sandwich materials for wind turbine blades - present and future", Journal of Sandwich Structures and Materials, Vol.11, p.p. 7-27, 2009.

[5] E.E. Theotokoglou and G.A. Balokas, Computational Analysis and Material Selection in Cross-Section of a Composite Wind Turbine Blade, Journal of Reinforced Plastics and Composites, 34(2): 101-115, 2015.

[6] ANSYS Engineering Analysis System. User's manual, Swanson Analysis System Inc., Houston, USA, 2007.

[7] F.M. Jensen, B.G. Falzon, J. Ankersen, H. Stang, Structural Testing and Numerical Simulation of a 34m Composite Wind Turbine Blade, Composite Structures, 76, 52-61, 2006.

[8] E.E. Theotokoglou and G.A. Balokas, A Micro-Scale Structural Response Comparison Between GFRP and CFRP Wind Turbine Blades, Proceedings of the 8th GRACM International Congress on Computational Mechanics, Volos, Greece, July 12-15 2015.

[9] N. Gaudern. and D. Symons, Comparison of Theoretical and Numerical Buckling Loads for Wind Turbine Blade Panels, Wing Engineering, Volume 34, No. 2, PP 193-206, 2010.

[10] T. Burton, Sharpe D., Jenkins N. and Bossanyi E., "Wind Energy Handbook", Wiley, USA, 1991.

[11] M. Grujicic, G. Arakere, E. Subramanian, V. Sellappan, A. Vallejo, M. Ozen, Structural-Response Analysis, Fatigue-Life Prediction, and Material Selection for 1MW

Horizontal-Axis Wind Turbine Blades, Journal of Materials Engineering and Performance, 19: 790-801, 2009.

[12] J.E. Zimmer, J.R. Cost, Determination of the Elastic Constants of a Unidirectional Fiber Composite using Ultrasonic Velocity Measurements, J.Acoust. Soc. Am. 47, 795, 1970.

[13] C. Praveen Shaju, T. Manikandan, S. Sai Balaji, Experimental Study on Environmental Exposure of Kevlar Epoxy Composites, International Journal of Emerging Technology and Advanced Engineering, Volume 3, Issue 10, October 2013.

[14] X. Chen, W. Zhao, X.L. Zhao and J.Z. Xu, Failure Test and Finite Element Simulation of a Large Wind Turbine Composite Blade under Static Loading, Energies 2014, 7, 2274-2297.

[15] Ashwill, Materials and Innovations for Large Blade Structures: Research Opportunities in Wind Energy Technology, 50th AIAA Structures, Structural Dynamics & Materials Conference Palm Springs, May, 2009.

[16] K. Cox, A. Echtermeyer, Structural design and analysis of a 10MW wind turbine blade, Energy Procedia 24: 194-201, 2012.